

Star Formation Histories of Dwarf Spheroidal and Dwarf Elliptical Galaxies in the Local Universe

Mira Seo¹ and Hong Bae Ann^{1*}

¹*Department of Earth Sciences, Pusan National University, Busan, 609-735, Korea*

Accepted XXX. Received YYY; in original form ZZZ

ABSTRACT

We present the star formation histories (SFHs) of early-type dwarf galaxies, dSphs and dEs, in the local universe within $z = 0.01$. The SFHs of early-type dwarf galaxies are characterized by pre-enriched, metal-poor old stellar populations, absence of moderately old stars that have ages of a few Gyr. There are some differences in the SFHs of dSphs and dEs. In particular, dSphs formed old ($\gtrsim 10$ Gyr old) metal-poor stars ~ 2 times more than dEs. The effects of reionization and feedback from supernova explosions are thought to be strong enough to remove the gas left, which prevent moderately old stellar populations in dSphs. In contrast, the ejected gas are not completely removed from dEs and fall back to ignite burst of star formation at a few Gyr after the first period of violent bursts of star formation, showing a suppression of star formation at lookback time ≈ 9.6 Gyr. The second peak of star formation at lookback time ≈ 4.5 Gyr in dEs produce moderately old stellar populations. Distinction between dSphs and dEs is useful to examine the SFHs of the early-type dwarfs since the cumulative SFHs are most closely related to their morphology. The stellar mass plays an important role in the SFHs of the early-type dwarfs as a driver of star formation, especially in galaxies with primordial origin.

Key words: galaxies – dwarfs – dwarf spheroidal galaxies – dwarf elliptical galaxies – stellar populations – SFH

1 INTRODUCTION

Dwarf galaxies are most abundant in the local universe. They are thought to be building blocks of more massive galaxies in the framework of Λ cold dark matter (Λ CDM) cosmology (Blumenthal et al. 1985; Navarro, Frenk & White 1997). Some dwarf galaxies survive to the present time as isolated galaxies or satellites of larger galaxies. Among dwarf galaxies, early-type dwarf galaxies such as dwarf spheroidal galaxies (dSphs) and dwarf elliptical galaxies (dEs) are of special interest because they could be primordial objects that evolved to the present form. It is also likely that they are transformed ones from late-type galaxies if they are observed in group/cluster environment where a variety of mechanisms that transform late-type galaxies to early-type dwarfs are operable (e.g., Fatahi et al. 2018, references therein).

Some early-type dwarf galaxies that have primordial origin are thought to be fossils of primordial galaxies whose star formation had quenched before or during re-ionization (Gutcke et al. 2022). The majority of stars in these galaxies have ages older than 10 Gyr with metallicities lower than $[\text{Fe}/\text{H}] \approx -2$ since re-ionization is thought to occur at $Z \approx 6$ (Becker et al. 2001). Quenching of star formation was driven by the mechanical feedback from supernova explosions followed by the

bursts of star formation at an early epoch of cosmic evolution. Mechanical energy from the supernova explosions blows out the gas from the primordial galaxies which have shallow potentials due to small masses (Vader 1986; Dekel & Silk 1986; Sclavadori, Ferrara & Schneider 2008). Examples of such fossil objects are the Sextans dwarf spheroidal galaxy in the LG (Bettinelli et al. 2018). The ultra faint dwarf spheroidal (UDF) Segue 1 is also supposed to be fossil object (Frebel et al. 2014; Webster, Frebel & Bland-Hawthorn 2016).

The dEs comprise the most abundant population of galaxy clusters such as the Virgo cluster (Binggeli, Sandage & Tammann 1985) while the dSphs are mostly found in the Local Group (LG). Whether they are morphologically distinct or not, they are mostly satellites of bright giant galaxies (Makarov et al. 2015; Ann 2017). In the Local Group, most satellites of the Milky Way (MW) and Andromeda (M31), located within ~ 300 kpc from their host galaxies, are dSphs (McConnachie 2012). They are thought to be accreted into the host galaxies earlier than ~ 6 Gyr ago (D’Souza & Bell 2021; Barmantloo & Kautun 2023) but Hammer et al. (2023) argued that most dwarfs of MW are newcomers based on energy arguments. Some of them could be primordial objects but the majority of them are thought to be transformed from gas-rich dwarf irregulars which lost their cold gas by tidal stripping (Moore et al. 1996; Moore, Lake & Katz 1998; Mayer et al. 2001a,b; Kravtsov, Gnedin & Klypin

* E-mail: hbann@pusan.ac.kr

2004; Paudel & Ree 2014; Kazantzidis et al. 2017; Fattahi et al. 2018) and/or ram pressure stripping (Gunn & Gott 1972; Abadi et al. 1999; Koppen et al. 2018). The spiral arm features revealed in the unsharp masked images of a number of dEs in the Virgo clusters (Jerjen, Kalnajs & Binggeli 2000; Lisker, Grebel & Binggeli 2006) support the transformed late-type galaxies as their origin. The gas-rich late-type galaxies can be deprived of their gas by ram pressure stripping (Gunn & Gott 1972) and starvation (Larson, Tinsley & Caldwell 1980).

Besides the favorable environment for morphology transformation for early-type dwarfs, there are some observations that support the non-primordial origin of dEs. They are the embedded spirals observed in some dEs (Jerjen, Kalnajs & Binggeli 2000; Barazza et al. 2002; Graham, Jerjen & Guzman 2003; De Rijcke et al. 2003; Lisker, Grebel & Binggeli 2006) and fast rotations which imply rotationally supported systems (Pedraz et al. 2002; Simien & Prugniel 2002; Geha, Guhathakurta & van der Marel 2003; van Zee, Skillman & Haynes 2004; De Rijcke et al. 2005; Chilingarian et al. 2009; Geha et al. 2010; Toloba et al. 2015; Penny et al. 2016) together with the blue-cored dEs, which implies presence of cold gas at the central regions of a significant number of dEs in the Virgo Cluster (Lisker et al. 2007; Hamraz et al. 2019). The presence of blue-cored dEs are also observed in the Fornax Cluster and Coma Cluster with much larger fractions (Hamraz et al. 2019). Actually, there are some HI gas-rich dEs in the Virgo Cluster (Conselice et al. 2003; Hallenbeck et al. 2012) and in the Fornax Cluster (Buyle et al. 2005). On the other hand, there has been no report on the embedded spirals in dSphs. Most dSphs are dispersion-supported systems except for some dSphs which are supposed to be formed by mergers (Lokas et al. 2014). But the paucity of rotation-supported dSphs does not necessarily admit that they are not transformed from late-type galaxies because the dwarf irregulars seem to be dispersion-supported (Wheeler, Pace & Bullock 2017).

A non-negligible fraction of dEs and dSphs are isolated early-type dwarf galaxies of which origins could be primordial objects because they have no chance to interact with other galaxies. A recent CMD analysis for the star formation history (SFH) of an early-type dwarf galaxy Sextans (Bettonelli et al. 2018) shows that the majority of the stellar component formed before the end of the reionization which is assumed to be fixed at ~ 12.77 Gyr (Becker et al. 2001). Existence of early-type dwarf galaxies whose cold gas was completely exhausted in the early phase of galaxy evolution suggests different gas-loss mechanisms. Examples of the proposed gas-loss mechanisms are photoevaporation (Barkana & Loeb 1999; Gnedin 2000; Shapiro, Iliev & Raga 2004), supernova (SN) feedback (Dekel & Silk 1986; Ferrara & Tolstoy 2000; Marcolini et al. 2006; Bovill & Ricotti 2009), interaction with gaseous filaments (Benitez-Llambay et al. 2013). Dissolving star cluster scenario (Assmann et al. 2013) is another way to explain the formation of isolated dSph galaxies.

There has been no consensus on the morphological classification of dwarf galaxies. Simple classification scheme is to divide them as early-type dwarfs and late-type dwarfs. Aside from the late-type dwarfs which are designated by dIrrs or dIIs, early-type dwarfs are frequently divided into two sub-types of galaxies, dEs and dS0s, where the former include their faint cousins dSphs (Sandage & Binggeli 1984). Most

studies (eg., Binggeli, Sandage & Tammann 1985; Lisker, Grebel & Binggeli 2006) used the dE/dS0 division for early-type dwarf galaxies following Sandage & Binggeli (1984) although the terminology dwarf spheroidals (dSphs) have been used for the satellite galaxies of the MW and M31. Kormendy & Bender (2012) also neglect the sub-type dSph in proposing a new scheme for morphological classification which extends the parallel sequence of van den Bergh (1976). They used Sph rather than dE to represent the early-type dwarfs which include dE and dS0 galaxies in Binggeli, Sandage & Tammann (1985) and considered that dSphs are merely a smaller version of dEs. Buta et al. (2015) also used the notation Sph to describe the dE/dS0 galaxies observed in the Spitzer Survey of Stellar Structure in Galaxies (S4G). On the hand, the Updated Nearby Galaxy Catalog (Karachentsev et al. 2013, UNGC) employed a different approach to classifying galaxies in the Local Volume (LV) within 11 Mpc. They distinguished dSphs from dEs but they used Sph rather than dSph to denote dSphs. They classify dwarf galaxies based on surface brightness and color. In their classification, dE and Sph galaxies are classified to have red colors but with different surface brightness: high surface brightness for dE and normal to extremely low surface brightness for Sph. For comparison, dS0 galaxies have normal surface brightness with red colors. Another example of dwarfs with high surface brightness is BCD but BCD galaxies have blue colors. The explicit use of dSph was made by Ann, Seo & Ha (2015) to represent early-type dwarf galaxies similar to dE but shallower gradient in surface brightness distribution. The luminosity and colors of dSphs are a little bit less luminous and bluer than dEs but the majority of dSphs are brighter than $M_r = -13$, which overlaps the luminosity range of dEs.

In contrast to the morphology classification grid proposed by Graham (2019) where dwarf elliptical galaxies are treated as merely small versions of normal early-type galaxies, the early-type dwarfs, dSphs and dEs, can be distinguished from giant elliptical galaxies by their surface brightness distribution, which is better represented by the Sérsic profile (Sérsic 1968) with $n = 1 - 3$ (Geha, Guhathakurta & van der Marel 2003; Seo & Ann 2022). There is a slight difference in the mean Sérsic index n between dSphs and dEs in the sense that dSphs have smaller n (Seo & Ann 2022) which leads to shallower surface brightness distribution of dSphs. In contrast to the most previous studies (eg., Binggeli, Sandage & Tammann 1985; Lisker, Grebel & Binggeli 2006; Kormendy & Bender 2012), we distinguish dSphs from dEs. One of the reasons why we distinguish dSphs from the dEs is that dSph galaxies are mostly dispersion-supported systems (Walker et al. 2009; Salucci et al. 2012) while a considerable fraction of dE galaxies is supported by rotation (Geha et al. 2010). Their origins might be different. The difference in luminosity of dEs and dSphs are apparent because there is no dEs fainter than $M_B \approx -13$, at least in the LG. However, In the luminosity ranges between $M_R = -13$ and $M_R = -16$, a significant fraction of early-type dwarf galaxies is thought to be dSphs according to their morphology (Ann, Seo & Ha 2015).

Since the morphology of a galaxy is an integral property that reflects the physical properties such as dynamical structure and stellar populations. The former property is revealed by the apparent shape and surface brightness distribution while the latter is reflected by the luminosity, color and metal abundance. Since the stellar population of a galaxy is deter-

mined by the SFH, galaxies with similar morphology may experience similar SFHs. Thus, we can expect a link between morphology and SFH of galaxies, although it is apparent that a considerable fraction of the satellite galaxies in the LG shows somewhat different SFHs for the same morphological type (Weisz et al. 2014a). Since the SFHs of the 40 dwarf satellites of the LG were derived from the color-magnitude diagrams obtained from HST imaging, their SFHs are thought to be precise enough to reveal fine details of the evolution of these galaxies. The different SFHs of the dSphs in the LG might be due to differences in mass and environment. The mass range of the LG dSphs inferred from the luminosity range of ~ 8 mag is large enough to drive different SFHs in the early stage of evolution. Lower mass dwarfs are likely to be quenched earlier by the supernova feedback (Dekel & Silk 1986; Ferrara & Tolstoy 2000; Marcolini et al. 2006; Bovill & Ricotti 2009) than higher mass dwarfs. It is also not surprising that the star formation of the satellites at smaller distances from the host galaxy (MW or M31) is quenched earlier than those at a large distance by the environmental effects of their host halos (Boselli et al. 2008; Penny et al. 2012; Zhou et al. 2020).

Thus, it is necessary to analyze the stellar populations of early-type dwarfs to derive their SFHs. The most accurate method to analyze the stellar populations of a galaxy is to compare observed color-magnitude diagrams (CMDs) of resolved stars with synthetic CMDs (Tolstoy, Hill & Tosi 2009, references there in). But this method has been applied mostly to dwarf galaxies in the LG (Monelli et al. 2010a,b; de Boer et al. 2012; Hidalgo et al. 2012, 2013; Weisz et al. 2014a; Gallart et al. 2015) because it requires deep imaging that reach the oldest main-sequence turn-off (MSTO). Up to now, most distant galaxies of which CMDs are deep enough to derive the oldest populations are limited within the local volume of 10 Mpc. Thus, it seems obligate to use integrated spectra of galaxies that are located outside the local volume of 10 Mpc. We used the population synthesis code STARLIGHT (Cid Fernandes et al. 2005) which has been widely used for spectra observed in the Sloan Digital Sky Survey (York et al. 2000, SDSS). Recently, there are a number of studies (e.g., Cid Fernandes et al. 2013), applying STARLIGHT to explore stellar populations across galaxies using the spectra obtained from integral-field spectroscopic observations such as the Calar Alto Legacy Integral Field Area Survey (Sanchez, Kennicutt & Gil de Paz 2012, CALIFA) and Mapping Nearby Galaxies at Apache Point Observatory (Bundy et al. 2015, MaNGA). Among others, the Cid Fernandes et al. (2013) and Riffel et al. (2021) are examples of using STARLIGHT to the stellar population of galaxies in CALIFA and in MaNGA, respectively.

We are wondering that the morphological differences observed in the bright early-type dwarf galaxies are caused by the SFHs which are supposed to be closely related to their origins. The connection between the SFHs and the structural properties is also expected because the spatial distribution of stellar populations determines the structure of a galaxy. The flatter surface brightness distribution of dSphs which corresponds to smaller Sérsic index n than dEs is thought to be caused by the shallow potential of the dSphs. We expect earlier quenching of star formation in dSphs than in dEs due to their mass difference. The difference in quenching epoch can be traced by the stellar populations.

Most previous studies of SFHs of dSphs and dEs using CMD analysis were confined to those in the LG (Hermendez, Gilmore & Valls-Gabaud 2000; Aparicio et al. 2001; Dolphin 2002; Carrera et al. 2002; Lee et al. 2009; Monelli et al. 2010a,b; de Boer et al. 2012; Hidalgo et al. 2012, 2013; Brown et al. 2014; Weisz et al. 2014a; Gallart et al. 2015; Savino, Salaris & Tolstoy 2015; Santana et al. 2016; Makarova et al. 2017; Skillman et al. 2017; Bettinelli et al. 2018, 2019; Savino et al. 2019; Weisz et al. 2019; Gallart 2021; Rusakov et al. 2021; Navabi et al. 2021) except for a few cases (e.g., Weisz et al. 2011; Cignoni et al. 2019, references therein). Weisz et al. (2011) derived SFHs of 60 dwarf galaxies from the ACS Nearby Galaxy Survey Treasury (ANGST). They are located within ~ 4 Mpc except for DDO 165 of which distance is 4.6 Mpc and masses in the range $M_* \sim 10^{5-11} M_\odot$. This is because the derivation of SFHs requires high-quality CMDs that can be obtained for the galaxies of which constituent stars can be resolved. Because of the low luminosity of dEs and dSphs, their SFHs derived from the color-magnitude diagrams are confined to those in the local volume, mostly those in the LG.

Population synthesis of the dwarf galaxies beyond the LG was performed for the 12 dSphs in Cen A group at a distance of 3.8 Mpc (Muller et al. 2021) using integrated spectra obtained from the MUSE integral field spectrograph mounted at UT4 of the VLT on Cerro Paranal, Chile (Bacon et al. 2010). The dSphs have old and metal-poor stellar populations and follow the stellar metallicity-luminosity relation defined by the dwarf galaxies in the Local Group.

Here, we report an analysis of the SFHs of the early-type dwarf galaxies listed in the catalogue of visually classified galaxies in the local ($z \lesssim 0.01$) universe (Ann, Seo & Ha 2015, CVCG). To derive the SFHs of the early-type dwarfs, we applied a population synthesis code STARLIGHT (Cid Fernandes et al. 2005) to the optical spectra of two sub-types of the early-type dwarf galaxies (dSphs and dEs) observed in the Sloan Digital Sky Survey (SDSS; York et al. (2000)).

The present paper is organized as follows. In Section 2, selection of sample galaxies and observational data are described. The method and basic results of this study are presented in Section 3. The cumulative SFHs of the dSphs and dEs are described in section 4. Discussion of the SFHs of the early-type dwarfs is given in Section 5. Summary and conclusions are given in the last section.

2 SAMPLE SELECTION AND DATA

2.1 Selection of dwarf spheroidals and dwarf ellipticals

We selected the two sub-types of early-type dwarf galaxies, dSphs and dEs, from the galaxies in the CVCG which provides detailed morphological types of 5638 galaxies located in the local universe. The galaxies listed in the CVCG are mostly taken from KIAS-VAGC (Choi, Han & Kim 2010) which is a value-added catalogue based on the Sloan Digital Sky Survey (SDSS) Data Release 7 (DR7). The CVCG supplements the original catalogue with galaxies brighter than $r = 14.5$ whose redshifts were taken from literature (Choi, Han & Kim 2010, references there in). The CVCG took about 1000 galaxies from the NASA Extragalactic Database (NED) which were not included in the KIAS-VAGC due to selection criteria adopted. Thus, the CVCG is nearly complete

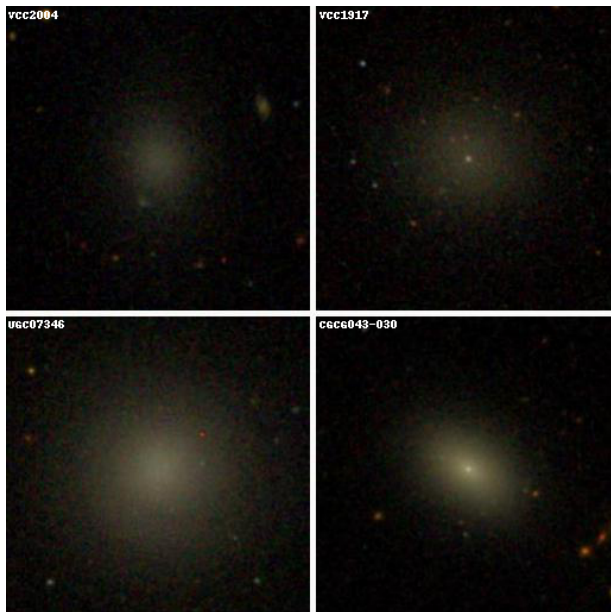


Figure 1. SDSS color images of four early-type dwarfs. Galaxies in the upper row are dwarf spheroidal galaxies and those in the lower row are dwarf elliptical galaxies. Left panels for non-nucleated dwarfs and right panels for nucleated dwarfs. The box size in one dimension is ~ 100 arcsec. North is up, and East to the left.

for galaxies brighter than $r = 17.77$ for the regions surveyed by the SDSS. [Ann, Seo & Ha \(2015\)](#) distinguished dSph and dE from other early-type morphology such as dS0 and dE_{bc}, which are dwarf lenticular galaxy and blue-cored dwarf elliptical galaxy, respectively. We confined our sample galaxies to dSphs and dEs for population synthesis studies because morphological features such as disc and lens are observed in dS0s and young stellar populations are dominant in the cores of dE_{bc} sub-types, which implies that they are not genuine primordial dwarfs although both of them are considered to be early-type dwarfs.

Figure 1 shows the color images of four sample galaxies, the upper row for dSphs and the lower row for dEs. We provide non-nucleated and non-nucleated dwarfs for each sub-type. Although the sub-types of early-type dwarfs are classified by the morphological characteristics ([Ann, Seo & Ha 2015](#)), there are some difference in luminosity and colors of dSphs and dEs. The luminosity difference between dEs and dSphs is apparent because there is no dEs fainter than $M_B \approx -13$, at least in the LG. For the present sample of dSphs and dEs, on average, dSphs are ~ 1.5 mag fainter than dEs. However, as shown in Figure 2, there is a range of luminosity, $M_r = -13 \sim M_r = -16$, where a significant fraction of dSphs and dEs are present. The majority of dSphs and dEs are located along the red sequence ([Strateva et al. 2001](#)) but some deviate a lot from it. The large spread in the $u-r$ colors of dSphs seems to be due to large photometric errors in u -band magnitudes which occurred frequently in faint galaxies.

2.2 Data

We used the SDSS spectra of the selected dSphs and dEs which were downloaded from the SDSS DR7. The SDSS spectra are obtained by fibers of $3''$ in diameter placed at the focal

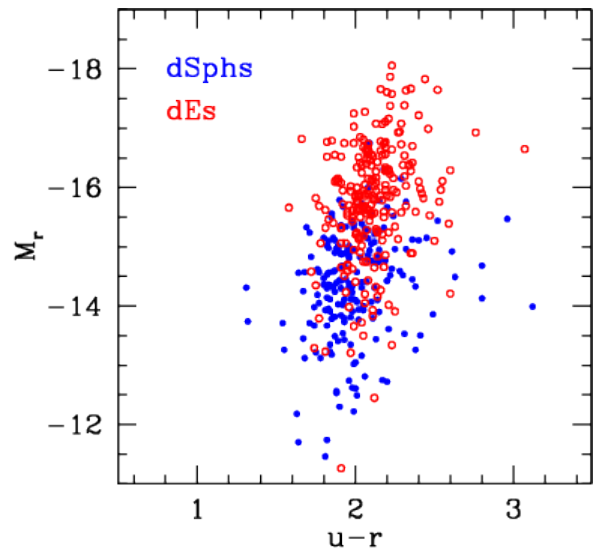


Figure 2. Color-magnitude diagram of early-type dwarf galaxies. Dwarf spheroidal galaxies are represented by filled blue circles and dwarf elliptical galaxies are plotted by open red circles.

plane of the 2.5 m telescope of the Apache Point Observatory. The SDSS spectrograph use 320 fibers with exposure time of 45 minutes or longer to achieve a fiducial signal-to-noise ratio. The spectra cover a wavelength range of 3800 to 9200 Å with a mean spectral resolution of $\lambda/\Delta\lambda \sim 1800$. The wavelength and flux are calibrated using pipeline developed by the SDSS team. Since the average effective radius (R_e) of the sample galaxies is $\sim 12''$ ([Seo & Ann 2022](#)), the spectra we use in the present study reflect the stellar populations in the central regions of sample galaxies, $\sim 13\%$ of R_e . We could obtain most of the spectra from SDSS DR7 but for a small fraction of sample galaxies ($\lesssim 5\%$), we did not find relevant spectra. We present the spectrum of one of dSphs whose r -magnitude is similar to the median values of the sample galaxies in Figure 3. The spectrum shows the typical features of early type dwarf galaxies. We use the observational data listed in the CVCG such as distance, luminosity (M_r), color ($u-r$), morphological type as well as coordinates and redshifts.

3 STAR FORMATION HISTORIES

3.1 Methods

We applied STARLIGHT ([Cid Fernandes et al. 2005](#)) to the SDSS spectra of 200 dSphs and 234 dEs to obtain the most probable mix of stellar populations as a function of stellar age and metallicity. The STARLIGHT, a synthesis code, is well described by [Cid Fernandes et al. \(2004, 2005\)](#) and a recent application is found in [Riffel et al. \(2021\)](#). It fits an observed spectrum with the model spectrum derived from a combination of N simple stellar population (SSP) based on the evolutionary synthesis models of [Bruzual & Charlot \(2003, BC03\)](#). BC03 provides spectral evolution of SSPs of various metallicities ($Z = 0.0001, 0.0004, 0.004, 0.008, 0.02, \text{ and } 0.05$) at ages between 1×10^5 and 2×10^{10} yr with a resolution of 3 Å across the wavelength range from 3200 to 9500 Å. They used the IMF of [Chabrier \(2003\)](#) with lower

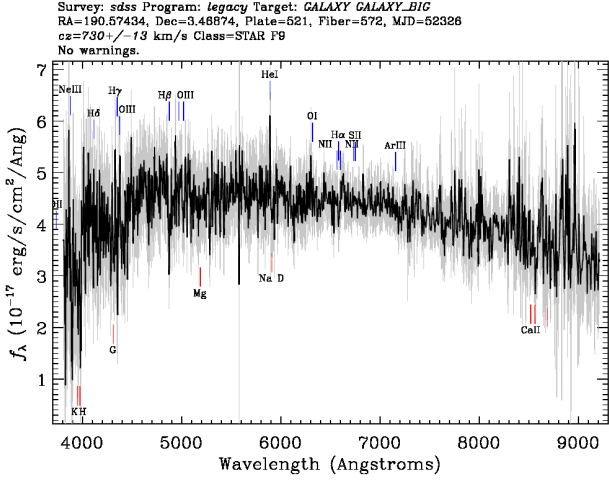


Figure 3. Spectrum of VCC 1917 adopted from SDSS DR7. Some absorption features are designated.

and upper mass cut-offs $m_L = 0.1M_\odot$ and $m_U = 100M_\odot$. The basic stellar evolutionary tracks are those from Padova groups complemented by Geneva groups with the STELIB library (Le Borgne et al. 2003).

In STARLIGHT, stellar motions projected to the line-of-sight are modeled by a Gaussian distribution (G) centered at radial velocity v with velocity dispersion σ . The extinction due to foreground dust is taken into account using the V-band extinction A_V . Thus, the model spectrum M_λ is expressed as

$$M_\lambda = M_{\lambda_0} \left(\sum_{j=1}^{N_*} x_j b_{j,\lambda} r_\lambda \right) \otimes G(v_*, \sigma_*) \quad (1)$$

where $b_{j,\lambda}$ is the j th SSP spectrum normalized at λ_0 , $r_\lambda = 10^{-0.4(A_\lambda - A_{\lambda_0})}$, M_{λ_0} is the synthetic flux at the normalization wavelength λ_0 , and x_j is the fractional contribution of the SSP for j th population that have age t_j and metallicity Z_j . The best fitting model is determined by selecting a model that minimizes the $\Xi^2 = \sum [(O_\lambda - M_\lambda) w_\lambda]^2$ where O_λ is observed spectrum and w_λ is the inverse of error applied (see Cid Fernandes et al. (2004) for detailed description).

Since STARLIGHT compares the model spectrum at rest frame, we corrected for the interstellar reddening and redshift before resampling the observed spectrum. The reddening correction was made by multiplying $10^{0.4A_\lambda}$ to the observed spectrum where A_λ is interstellar extinction at λ . We derived A_λ by using the reddening law of Cardelli et al. (2010) with $E(B-V)$ obtained from the dustmaps (Schlegel, Finkbeiner & Davis 1998) by assuming the total-to-selective extinction ratio (R_V) of 3.1. After reddening correction, we shifted the observed wavelength to the rest frame wavelength using the relation $\lambda_{rest} = \lambda_{obs}/(1+z)$ where z is the redshift. We also applied the dimming of the flux due to cosmic expansion by multiplying $(1+z)^3$ to the reddening corrected flux. We resampled the corrected spectrum with a sampling width of $\delta\lambda = 1 \text{ \AA}$ by applying a linear interpolation between the two nearest data points for the STARLIGHT input spectrum.

For the analysis of the star formation histories, STARLIGHT provides luminosity fraction (x_j) and mass

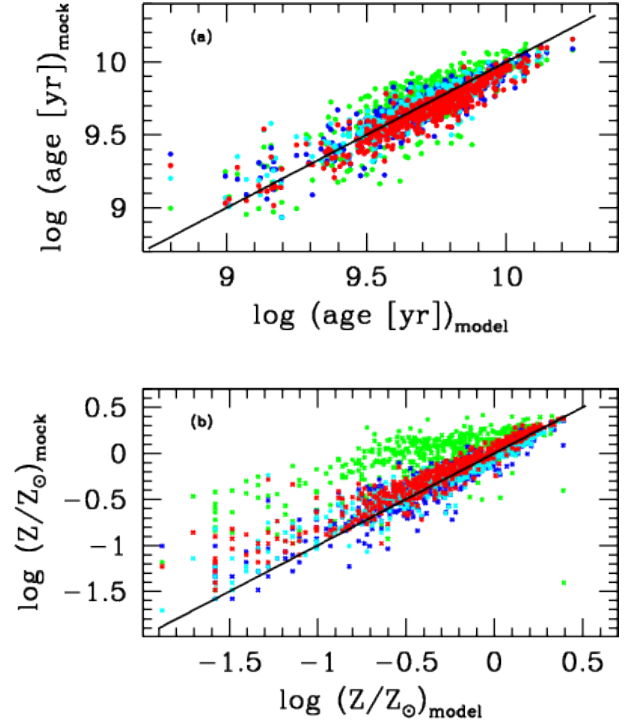


Figure 4. Mock test with $S/N = 5, 10, 20, 30$. The colors are assigned to distinguish S/N : 5 (green), 10 (blue), 20 (cyan), and 30 (red). The black solid lines are one-to-one relation lines.

fraction (μ_j) for j -th stellar population as a function of stellar age. The x_j and μ_j are divided into six stellar metallicities ($Z = 0.0001, 0.0004, 0.004, 0.008, 0.02, \text{ and } 0.05$). It assumes $[\alpha/\text{Fe}] = 0$. The output of STARLIGHT gives two mass fractions, μ_{ini} and μ_{cor} , which represent initial mass and mass corrected for the mass returned to the interstellar medium, respectively. We used the μ_{cor} for the mass fraction of stellar populations while we used the μ_{ini} to derive the star formation rates.

3.2 Mock spectra with noises from a Gaussian perturbation

We applied STARLIGHT to the mock spectra to test the robustness of the stellar populations we derived. We constructed the mock spectra using the model fluxes from the STARLIGHT output which fits the observed spectra of sample galaxies. The flux of a mock spectrum is calculated as

$$F(\lambda) = F_{model}(\lambda) + F_{model}(\lambda)/(S/N) \times G(\lambda) \quad (2)$$

where $G(\lambda)$ is a number randomly drawn from a Gaussian normal distribution $N(0, 1^2)$ at wavelength λ (Eq. 6 of Wang et al. (2022)). We used four signal-to-noise ratios (S/N) of 5, 10, 20, and 30, which well cover the S/N of the observed spectra of sample galaxies. The total number of mock spectra is 1736 since four mock spectra were constructed for each model flux of 434 early-type dwarf galaxies.

Figure 4 shows the mean ages and metallicities of mock galaxies compared with those of model galaxies whose stellar populations were determined from the observed spectra of sample galaxies using STARLIGHT. As shown in Figure

4-(a), the method we employed to determine the stellar populations seems to well reproduce the ages of mock galaxies of which spectra were perturbed by noises proportional to S/N^{-1} . The metallicities of mock galaxies are also well reproduced except for those from mock spectra with $S/N = 5$. As shown in Figure 4-(b), they are overestimated by ~ 0.3 dex for solar metallicity and ~ 0.7 dex for metallicities of $\log(Z/Z_{\odot}) < -0.5$. It implies that the metallicity determination is more affected than the ages by spectral noises. It seems to be partially due to incomplete templates in BC03 SSPs and the resemblance of the SSP spectra for the old metal-poor populations in BC03.

However, the ill reproduction of metallicities from the mock spectra that have $S/N = 5$ is not a severe problem for the present study because most SDSS spectra of the sample galaxies have S/N greater than 5. It is also worth to note that the fluxes at wavelengths with large errors are masked during the fitting process in STARLIGHT so that the best fitted model fluxes are not much affected by the large errors in the observed fluxes which result in the small S/N .

3.3 Stellar Mass

The stellar masses of sample galaxies are calculated from the model fluxes determined by STARLIGHT using the distances in the CVCG. They are mostly in the range of $10^6 \sim 10^8 M_{\odot}$. But they are not the total stellar masses of galaxies because they are calculated from the model fluxes fitted to the observed spectra through the $3''$ fiber which covers a small fraction of a galaxy image. In order to obtain the total stellar mass, we applied aperture correction (AC) calculated as

$$AC = \frac{2 \times \int_0^{R_e} f(r) dr}{\int_0^{R_f} f(r) dr} \quad (3)$$

where R_e and R_f are the effective radius and the fiber radius, respectively, and $f(r)$ is the Sérsic profile (Sérsic 1968). We use the R_e and Sérsic index (n) that were determined by Seo & Ann (2022). For galaxies with unknown R_e and n , we use the mean R_e and n derived for dSphs and dEs. They are $R_e \approx 12''$ and $n \approx 0.9$ for dSphs and $R_e \approx 11''$ and $n \approx 1.3$ for dEs, respectively. The number of galaxies with unknown Sérsic parameters is $\sim 10\%$ of the sample galaxies. The stellar masses of dSphs are on average 4 times smaller than those of dEs, which corresponds to a magnitude difference of $\Delta m = 1.5$ if we assume the same mass-to-luminosity ratio for both types. This magnitude difference is consistent with the magnitude difference shown in Figure 2.

Figure 5 shows a comparison between the present estimates of the total stellar mass and those from SDSS DR12. The total stellar masses provided by SDSS DR12 were derived from multi-band photometric images following Kauffmann et al. (2003) and Brinchmann et al. (2004). About 10% of sample galaxies are missed in the stellar mass table of SDSS DR12. In particular, $\sim 20\%$ of dSphs are missed in the SDSS DR12. There is a good correlation between the two sets of stellar masses. There are some outliers in the stellar masses from SDSS DR12 as well as the present estimates. We suppose that the outliers are mostly caused by large errors in the distances of galaxies because most of the distances are derived from the redshifts. In particular, the stellar masses larger than $10^{10} M_{\odot}$ are thought to be due to the larger distances applied to these

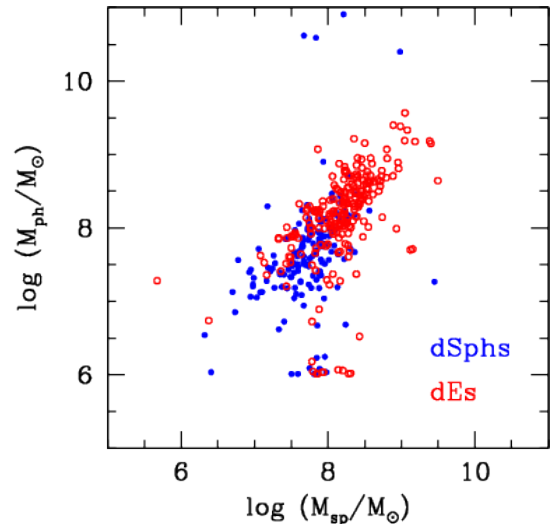


Figure 5. Comparison of the stellar mass from STARLIGHT corrected for fiber aperture and the stellar mass from SDSS DR12. The horizontal axis for the stellar mass from STARLIGHT (M_{sp}) and the vertical axis for the stellar mass from SDSS DR12 (M_{ph}). Dwarf spheroidal galaxies are represented by filled blue circles and dwarf elliptical galaxies are plotted by open red circles.

galaxies. However, the tight correlation for the majority of sample galaxies is remarkable because the two approaches are completely independent. This confirms the robustness of the population synthesis applied in this study.

3.4 Luminosity and Mass Fraction

Figure 6 and 7 show the mean luminosity and mass fractions of the stellar populations as a function of stellar age for dSphs and dEs, respectively. We applied sigma clipping that excludes galaxies deviate more than 3σ from the mean. The number of rejected galaxies is less than $\sim 3\%$ of the whole sample. The SFHs of 200 dSphs and 234 dEs are provided in supplemented material as a tabular form, respectively. Some galaxies formed the majority of stars at early epochs of $\log(t_L) \gtrsim 10$ where t_L is the lookback time in unit of yr, while others form most stars at later times, $\log(t_L) < 10$. The general trend of SFHs of the early-type dwarfs is the multiple bursts of star formation with decreasing strength toward the present time. The active periods of star formation ended just after $\log(t_L) \approx 9$ and resumed at $\log(t_L) \approx 8$ with much more reduced strength. The period of quenched star formation between $\log(t_L) \approx 9$ and 8 is frequently observed in the SFHs of the early-type dwarfs in the LG (Tolstoy, Hill & Tosi 2009). The recent star formation, which is virtually negligible in stellar mass fractions, is marginally noticeable in luminosity fractions due to the high luminosity of young massive stars. There is not much difference between dSphs and dEs for the SFHs after $\log(t_L) \approx 8$.

The most notable feature of the SFHs of early-type dwarfs is the presence of two periods of active star formation. The first period is peaked at $\log(t_L) = 10$ and the second period occurs at $\log(t_L) = 9.4$. There are some differences in the characteristics of the double peaks between dSphs and dEs. In dSphs, the peak of the first period is ~ 6 times higher than

that of the second period in stellar mass fractions and ~ 3 times higher in luminosity fractions, whereas similar strength in stellar mass fractions and reversed fractions in luminosity for dEs. It is apparent that majority of stars in dSphs are the stars formed in the first period. They contribute $\sim 80\%$ of the present stellar mass and $\sim 55\%$ of the present luminosity. More than 80% of their mass is contributed by the stars older than ~ 10 Gyr. The difference in the strength of the initial bursts is thought to be due to the difference in the effect of stellar feedback which depends on the mass of galaxies. In our sample of early-type dwarfs, dEs are, on average, 4 times more massive than dSphs.

The difference in the fraction of stars in the second period of active star formation between dSphs and dEs is also related to the mass dependent stellar feedback. The stars formed in the second period of active star formation in dSphs is only half of that in dEs. This difference is thought to be caused by the different influence of stellar feedback due to their mass difference. The strong suppression of star formation after the initial starbursts in dSphs is caused by supernova feedback which heats and expels the gas left to the halo. The almost complete removal of gas in less massive dSphs is due to the explosive starbursts in the early phase of galaxy formation. The lower mass of dSphs also provides a favorable condition for gas removal in the low mass dSphs. The reionization feedback also plays a considerable role for the gas removal in low mass dSphs because reionization feedback is more effective in low mass galaxies (Dawoodbhoj et al. 2018).

The general behavior of star formation after the second period of star formation in dSphs is similar to that of dEs. It is characterized by a short period of quenched star formation until $\log(t_L) \approx 8$ followed by increasing star formation activity toward the present time. However, the total percentage of mass contribution by stars younger than ~ 0.1 Gyr is less than 5%. The almost quenched star formation between $\log(t_L) \approx 9$ and 0 resulted in the absence of intermediate-age stars older than ~ 0.1 Gyr. This feature of a highly suppressed star formation of intermediate age stars is also observed in some early-type dwarfs in the LG (Weisz et al. 2014a). The suppression of star formation is thought to be caused by stellar feedback such as supernova explosion and stellar wind. The cold gas of galaxies was heated and easily expelled to the halo of early-type dwarfs. After that, star formation was resumed and continued to the present time with multiple starbursts to produce young stellar populations which contribute $\sim 5\%$ of the present luminosity and $\lesssim 0.2\%$ of the stellar mass in total. The resumed star formation at $\log(t_L) \approx 8$ is thought to be driven by the accretion of cold IGM because the metallicities of stars formed just after the period of quenched star formation can be explained if we assume accretion of metal free IGM as described below.

3.5 Metallicity Dependent Mass Fractions

3.5.1 Dwarf Spheroidal galaxies

Figure 8 shows the mean mass fractions of the stellar populations of 200 dSphs, divided into 6 metallicity groups, as a function of stellar age. As described above for the derivation of mean luminosity and mass fractions, we applied a sigma clipping method to exclude outliers. The stellar metallicities we used are $Z = 0.0001$, $Z = 0.0004$, $Z = 0.004$, $Z = 0.008$,

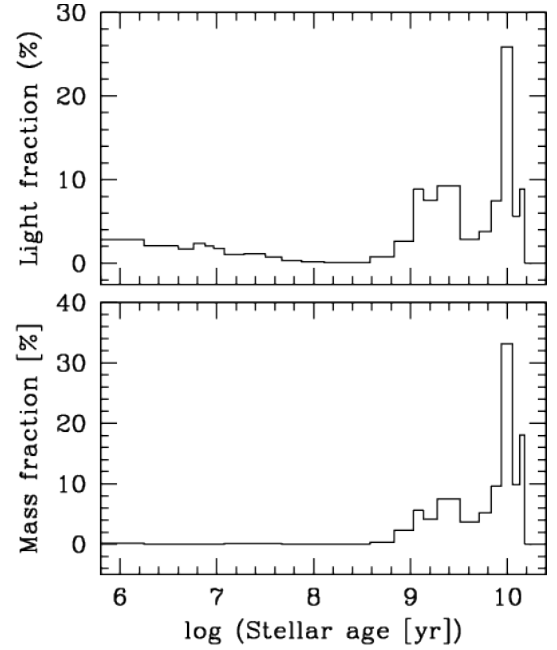


Figure 6. Mean luminosity and mass fractions as a function of stellar age for 200 dwarf spheroidal galaxies.

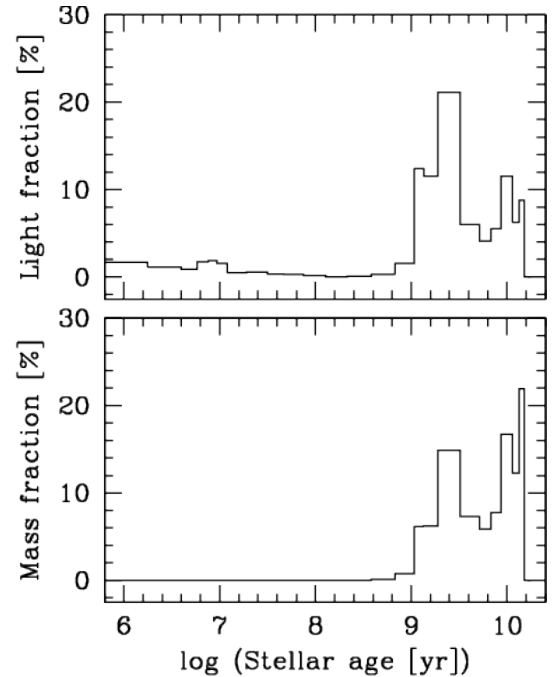


Figure 7. Mean luminosity and mass fractions as a function of stellar age for 234 dwarf elliptical galaxies.

$Z = 0.02$, and $Z = 0.05$. The most pronounced feature of the SFH of dSphs is the explosive star formation at $\log(t_L) = 10$ which produced $\sim 40\%$ of the present stellar mass. More than 99% of them are metal poor ($Z = 0.0004$) stars and the rest have metallicities of $Z = 0.0001$ and $Z = 0.004$ with negligible fractions.

The first period of star formation continued to form metal-

poor stars until $\log(t_L) \approx 9.8$ and contributes 80% of the present stellar mass. In terms of luminosity, the metal poor stars formed in the first period of star formation contribute 54% to the present luminosity. Since the majority of the oldest stars formed at $\log(t_L) \gtrsim 10$ have a metallicity of $Z = 0.0004$, which corresponds to $[\text{Fe}/\text{H}] = -2.6$ assuming the solar abundance of 0.01524 (Bressan et al. 2012), the first generation stars in dSps are assumed to be formed from pre-enriched gas. The metals from stellar evolution enriched the gas left, but a larger fraction of metals was thought to be ejected into the halo (Emerick et al. 2019). We expect some halo metal fell back to the nuclear region to enrich the gas left further.

The metallicity distribution of the stars formed in the second period of the active star formation is much different from that of the first period. A variety of metallicities from $Z = 0.0001$ to $Z = 0.05$ are involved in the stars formed in the second period. It begins with $Z = 0.004$ at the beginning of the second period and increases with decreasing stellar age nearly monotonically. At the end of the second period at $\log(t_L) \approx 8.9$, the metallicity of stars becomes $Z = 0.05$. As the stellar ages become younger, the metallicity of stars increases to become $Z = 0.05$ at the end of the second period. The dominant stellar populations of the second period of active star formation are stars of intermediate metallicity ($Z = 0.004$ and $Z = 0.008$), with a slightly higher fraction of $Z = 0.008$.

The stellar populations formed in the second period of star formation contribute 20% of the present stellar mass. Among the stellar populations formed in the second period, the mass of the extremely metal-rich stars is $\sim 4\%$ of the present stellar mass. The presence of a considerable amount of metal-rich populations suggests that a rapid chemical evolution had occurred in the majority of dSphs.

The third period of star formation, from $\log(t_L) \approx 8$ to the present time, shows several episodes of a starburst with very weak intensity. The stars in this period have a variety of metallicity, from $Z = 0.0001$ to $Z = 0.05$ with a large contribution of extremely metal poor stars formed at $\log(t_L) \approx 6.7$. These bursts produced stars that contribute negligible fractions ($\lesssim 0.1\%$) to the present stellar mass.

Since there is negligibly small amount of extremely metal-poor stars formed in the first and second periods of star formation in dSphs, the extremely metal-poor stars formed recently could not be formed from the gas that fell into the potential well of the dark matter halo in the early phase of its formation. Rather, they were formed from the gas that came in recently from the surrounding cold IGM because the metallicity of the gas in the nuclear regions of a galaxy increases monotonically unless pristine IGM is accreted onto the nuclear regions. The presence of HI gas around galaxies is well established (Danforth & Shull 2008) with more frequent in field galaxies than in group galaxies (Wakker & Savage 2009). However, there are two possibilities for the origin of the gas out of which the stars that have metallicities higher than $Z = 0.0001$ form. One is that it is the gas ejected into the halo of dSphs which cooled and settled down into the nuclear regions of the galaxy to form stars. The variety of metallicity for the young stellar populations can be explained if the metals ejected into the halo do not distribute uniformly. The other is that it is the cold IGM which is inhomogeneously mixed with the metals in the halo of the galaxy. Since dSphs are mostly consisted of old stellar populations (Gallagher &

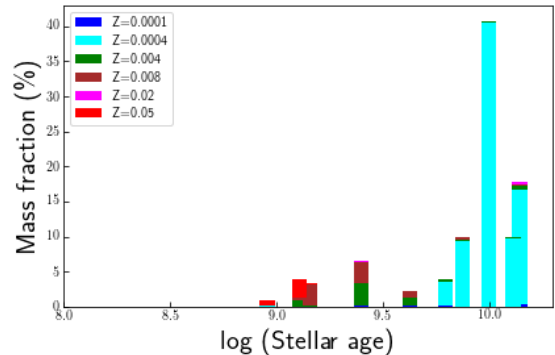


Figure 8. Mean mass fractions of stellar populations as a function of stellar age for 200 dwarf spheroidal galaxies. Stellar populations are divided by their metallicities.

Wyse 1994; Grebel, GaLLagher & Harbeck 2003) and they do not have cold gas out of which stars form. These young stellar populations are thought to be formed from the accreted IGM. In any case, the accretion of IGM played an important role because it seems to be metal free, which is required to produce the extremely metal-poor stars.

3.5.2 Dwarf Elliptical galaxies

The mean SFH of dEs, divided according to stellar metallicity as a function of stellar age, is presented in Figure 9. The characteristics of SFH, distinguished by stellar metallicities, are much different from that of dSphs shown in Figure 8. First of all, the early bursts occurred at $\log(t_L) \gtrsim 10.1$ is very explosive that made rapid metal enrichment of the interstellar medium from which generations of stars form. The explosive star formation of the initial burst is already seen in Figure 7, but here we see a rapid chemical evolution at the earliest phase of galaxy formation. The explosive bursts at $\log(t_L) \gtrsim 10.1$ produced four kinds of metallicity, from $Z = 0.0004$ to $Z = 0.05$ but the contribution by the extremely metal rich ($Z = 0.05$) stars is negligibly small, $\sim 0.3\%$. It seems difficult to consider the presence of extremely metal rich stars as a real feature since it requires an unusually large number of cycles of star formation. If it is a real feature, there is an extremely inhomogeneous mixing of metals to make extremely metal rich stars. Pre-enrichment may have some role for rapid metal enrichment. The fraction of metal rich ($Z = 0.02$) stars is considerable enough to confirm a rapid chemical evolution in dEs although the majority of stars formed in the first period of active star formation are metal poor stars.

The chemical evolution of dEs during the second period of star formation is similar to that of dSphs, that is, it started with intermediate metallicities ($Z = 0.004$ and $Z = 0.008$) and ended with extremely metal rich stars. The most dominant metallicity in the second period of star formation is higher intermediate metallicity ($Z = 0.008$) which amounts to more than half of stars formed in the second period. The larger contribution of stars with $Z = 0.008$ than dSphs is due to the more rapid enrichment in dEs. Owing to rapid enrichment, extremely metal rich stars are found over a large range of stellar ages. Virtually, all generations of stars formed in the first and second periods of star formation have extremely metal rich stars, although they contribute to the present stel-

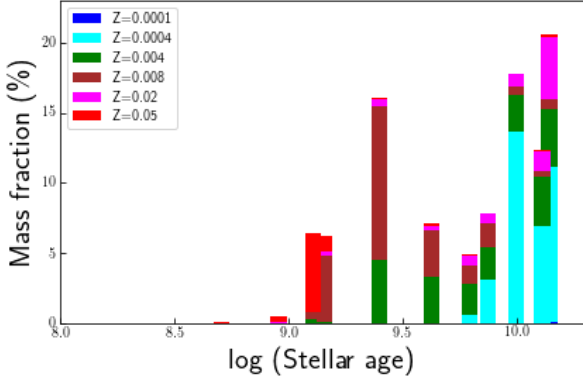


Figure 9. Mean mass fractions of stellar populations as a function of stellar age for 234 dwarf elliptical galaxies. Stellar populations are divided by their metallicities.

lar mass negligibly small except for the stars formed in the late phase of the second period at $\log(t_L) \approx 9.1$.

Aside from the pronounced differences between dEs and dSphs, one notable difference in SFHs between dEs and dSphs is observed in the fractions of the extremely metal poor ($z = 0.0001$) stars. The contribution of the extremely metal poor star to the present stellar mass is less than 1% in dEs while that in dSphs is slightly larger than 2%. This difference is more pronounced in the fractions of the oldest populations which contribute the highest fractions to the extremely metal poor stars. The extremely metal poor stars in the oldest population of dEs contribute only 0.2% of the present stellar mass while those of dSphs contribute 0.8%.

The metallicity distribution of stars formed after the second period of star formation is not much different from that of dSphs. There is a very weak star formation after the end of the second period at $\log(t_L) \approx 8$. Only $\lesssim 0.2\%$ of the present mass was formed after the second period.

4 CUMULATIVE STAR FORMATION HISTORIES

We derived the cumulative star formation history (cSFH) of dSphs and dEs to examine the mass assembly history of early-type dwarf galaxies. We analyzed two parameters related to the cSFH. One is the epoch of maximum starburst which shows the formation time of the dominant stellar population. The other is the quenching time which is defined as the lookback time when most of the galaxy mass is assembled. There are some advantages to use cSFH rather than SFH because cSFH circumvents the uncertainties derived in the absolute SFHs (Joshi et al. 2021) as well as suppresses the noise caused by the limited resolution of stellar ages.

4.1 Epoch of Maximum Star Formation

It is well known that there is a bi-modality in the age of stellar populations of galaxies demonstrated by two peaks in the galaxy age distribution (Gallazzi et al. 2005, 2008). One peak is caused by the old early-type galaxies and the other peak by young star forming galaxies. The distribution of stellar ages presented in Figures 6 - 9 strongly suggests a bi-modality of star formation in early-type dwarf galaxies, especially in

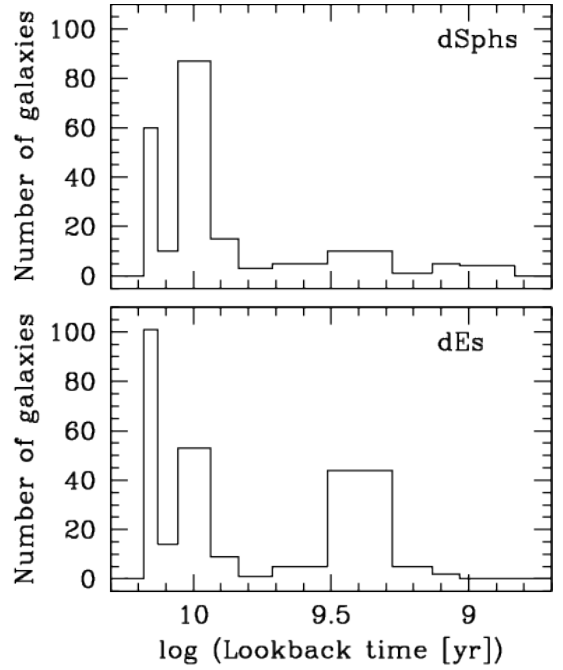


Figure 10. Frequency distribution of the epochs of maximum starbursts.

dEs. The reason for a weak bi-modality in the SFHs of dSphs seems to be due to feedback of supernova explosion which heats the cold gas to blow out (Dekel & Silk 1986). Figure 10 shows the distribution of epochs of starbursts. It is clear that star formation in early-type dwarfs is not a single event but multiple episodes of starbursts. The first epoch of starbursts occurs at $\log(t_L) \gtrsim 10.1$ for both dSphs and dEs. This epoch includes the first and second bursts shown in Figures 6 - 9. The fraction of galaxies which form stars at the first epoch of starburst is about 30% of dSphs and 43% of dEs, respectively. The first epoch of starburst is the second-high peak in dSphs while it is the highest peak in dEs. The 86% of dSphs and 76% of dEs result in starbursts during the first period of star formation. The highest peak of the second period of star formation in dSphs occurs at $\log(t_L) \approx 9.4$. This peak is made of 10 dSphs only. Thus, the bi-modality of star formation in dSphs is very weak compared to that of dEs of which 44 galaxies ($\sim 20\%$) have starbursts at this epoch. There are some bursts of star formation after the second period of star formation in dSphs, but it occurs in $\sim 2\%$ of dSphs. It is greatly contrasted with the bi-modality of star formation commonly observed in starburst galaxies (Cid Fernandes 2018).

4.2 Quenching Epoch

In past studies of the SFHs of galaxies, it is a common practice to present the characteristics of SFHs in a graphical form such as the figures in the previous sections. Weisz et al. (2014a,b, 2015) introduced a parameter, quenching time τ_{90} , which is defined as the lookback time at which 90% of stellar mass is formed, to quantify the cSFHs of galaxies. Figure 11 shows the histograms of τ_{90} for the 200 dSphs and 234 dEs. As expected from the difference in SFHs of dSphs and

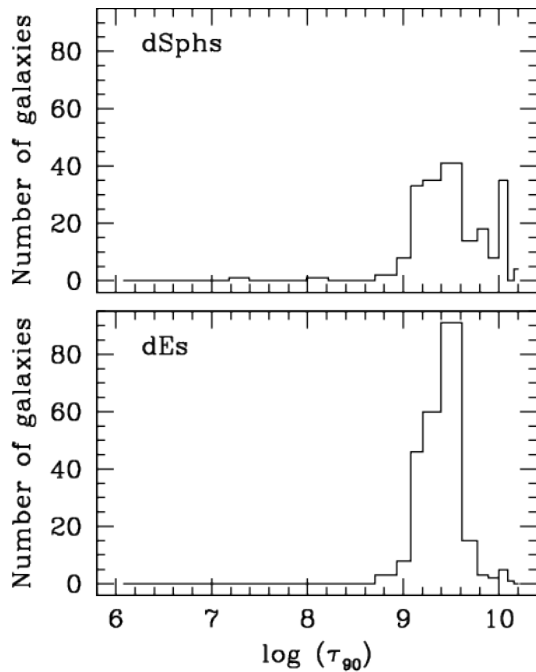


Figure 11. Frequency distribution of quenching time τ_{90} .

dEs shown in the above, there is a clear difference in the distribution of τ_{90} . In particular, a significant fraction of dSphs have $\log(\tau_{90}) > 10$ while only a negligible fraction of dEs have $\log(\tau_{90}) > 10$. The extremely early quenching of $\sim 20\%$ of dSphs is thought to be due to small mass of these galaxies since low mass dwarfs are known to be quenched earlier (Digby et al. 2019; Garrison-Kimmel et al. 2008; Joshi et al. 2021). Besides it, there are two other differences between the dSphs and dEs. One is the highly concentrated distribution of τ_{90} in dEs compared with the broad distribution of τ_{90} in dSphs. In both dSphs and dEs, the peak, i.e., the maximum frequency, occurs at $\log(t_L) \approx 9.7$, but the peak height is ~ 2 times higher in dEs than dSphs. The other is that virtually no dEs have $\log(\tau_{90})$ less than 8. It seems highly probable that the dSphs with $\log(\tau_{90}) > 10$ are bona fide primordial objects. The paucity of such early quenched dEs may imply that most of dEs are not primordial objects.

4.3 Dependence on Morphology, Stellar Mass and Environment

We investigated the dependence of cSFHs on the morphology, stellar mass, and environment of early-type dwarfs. We used the present estimates of the total stellar mass and the local background density derived from the data in the CVCG.

4.3.1 Morphology

Figure 12 shows the cSFHs of early-type dwarfs as a function of lookback time, grouped by the two morphological types, dSph and dE. We selected galaxies with the local background density around the median density (Σ_m), i.e., $\Sigma_m - 1\sigma < \Sigma < \Sigma_m + 1\sigma$ to avoid the effect of the local background density on the cSFHs. We present the mean cSFHs and $\pm 1\sigma$ boundaries. There is a significant difference in the cSFHs between dSphs

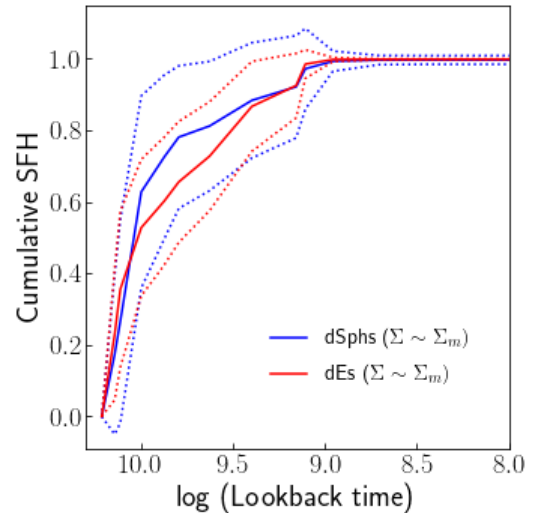


Figure 12. Cumulative SFHs of dSphs and dEs. We selected galaxies with the local background density, $\Sigma_m - 1\sigma < \Sigma < \Sigma_m + 1\sigma$ where Σ_m and σ is the median and standard deviation of the local background density, respectively. We plot the mean cSFHs of dSphs (blue solid line) and dEs (red solid line) together with 1σ boundaries (dotted lines).

and dEs from $\log(t_L) \approx 10$ to $\log(t_L) \approx 9.5$. It amounts to $\sim 0.8\sigma$ from the mean cSFH of dEs at $\log(t_L) \approx 9.8$. This difference is mainly due to the explosive bursts of star formation in dSphs at $\log(t_L) \approx 10$, as shown in Figure 8. It causes a rapid increase in cSFH of dSphs after $\log(t_L) = 10$. Owing to the rapid assembly of stellar mass in early-type dwarfs, it becomes 62% of the present stellar mass in dSphs and 52% of the present stellar mass in dEs at $\log(t_L) = 10$.

The evolution of cSFHs of dSphs and dEs shows three characteristic features. The first feature is the very steep slopes of dSphs and dEs at $\log(t_L) \gtrsim 10$. Both types have nearly the same slopes in this period. The second feature is the significant difference in the cSFHs in the second period of star formation from $\log(t_L) \approx 9.7$ to $\log(t_L) \approx 9$. There is a break in the cSFH of dSphs while dEs have a nearly constant slope. The slope before the brake at $\log(t_L) \approx 9.8$ is similar to that of dEs while the slope after the brake is shallower than that of dEs. The cSFHs are nearly constant after $\log(t_L) \approx 9$ for both types due to quenching at $\log(t_L) \approx 9$.

As can be inferred from the 1σ upper boundary of the cSFH of dSphs in Figure 12, a significant fraction of dSphs make $\sim 90\%$ of their stars during the first period of star formation. This is one of the reasons why we think most of dSphs are primordial objects while a significant fraction of dEs are transformed ones.

4.3.2 Stellar Mass

As can be seen in Figure 5, it is apparent that dSphs and dEs have different stellar mass distributions. The distinction of cSFH of dSphs from that of dEs shown in Figure 12 may be caused by the different stellar masses of the two types. Thus, it is of interest to see which is the main cause of the different cSFHs of the two types. There are two ways to separate the effects of morphology and stellar mass. One is to examine

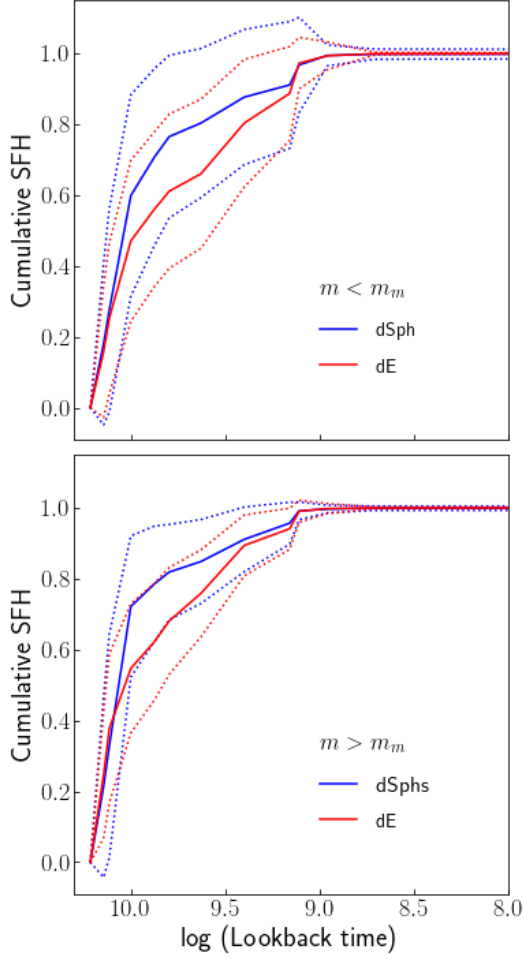


Figure 13. Cumulative SFHs of dSphs and dEs for the two stellar mass groups divided by the median mass of the whole sample which is $5 \times 10^7 M_\odot$. The cSFHs of galaxies in the low mass group are plotted in the upper panel and those of the high mass group are presented in the lower panel. The cSFHs of different morphology are distinguished by colors: dSphs (blue), dEs (red).

the dependence of cSFHs of the two types by constraining the stellar mass, and the other is to see dependence of cSFHs on the stellar mass by fixing the morphological type. To do this, we used the stellar masses of galaxies determined by population synthesis using STARLIGHT, corrected for the fiber aperture.

Figure 13 shows the dependence of cSFHs of early-type dwarfs on their detailed morphology. We divide the sample galaxies in two mass groups using the median stellar mass of the whole sample ($\sim 5 \times 10^7 M_\odot$). It is clear that the cSFH of dSphs is much different from that of dEs, regardless of their masses. Of the two mass groups, the high mass group shows more significant difference than the low mass group as the cSFHs of the two types differ about 1σ from others, which results in the probability of the K-S test as small as $p = 0.03$. The feature seen in Figure 12, i.e., more rapid star formation in dSphs than dEs, is confirmed here. The stellar mass dependence of cSFHs can be seen if we compare the cSFHs for the low mass group with those for the high mass group. The difference between low mass group and high mass

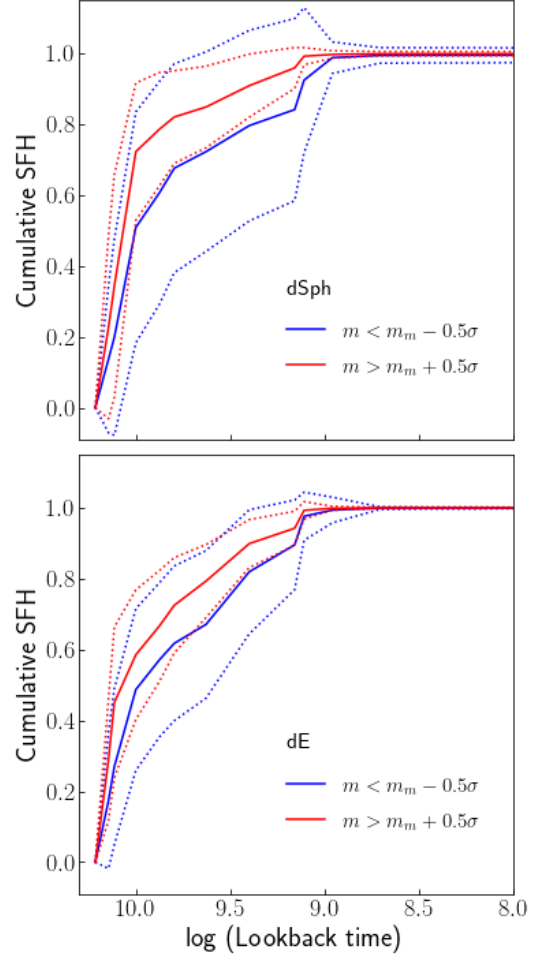


Figure 14. Cumulative SFHs of dSphs and dEs for the two stellar mass groups. Galaxies in the low mass group have total stellar mass (m) less than the median mass (m_m) - 0.5σ and those in the high mass group have m greater $m_m + 0.5\sigma$. Here, m_m is the median mass calculated for each type. Upper panel presents the cSFHs of dSphs and lower panel displays those of dEs.

group is more pronounced in the cSFH of dSphs than dEs. It suggests that the SFHs of the low mass early-type dwarfs are more affected by the stellar mass than that of the high mass early-type dwarfs. Since morphology is closely related to the SFHs of early-type dwarfs regardless of their masses, together with a moderate dependence of cSFHs of dEs on stellar mass, morphology seems to be more important in the SFHs of early-type dwarfs than the stellar mass.

Figure 14 shows the dependence of cSFHs of dSphs and dEs on the stellar mass. It is apparent that the cSFHs of both types depend on the stellar mass with somewhat stronger dependence in dSphs. Here we used two mass groups separated by 1σ difference in their total stellar mass. The cSFH of dSphs in the high mass group is $\sim 60\%$ higher than that of the low mass group until $\log(t_L) = 10$. The difference in the cSFHs between the low mass dSphs and the high mass dSphs becomes largest at $\log(t_L) \approx 10.1$, and decreases smoothly until $\log(t_L) \approx 8.7$. Thereafter, the two cSFHs are almost the same. The cSFH of the low mass dSphs is similar to the lower 1σ boundary of the cSFH of the high mass dSphs. The K-S

test shows that the two groups are significantly different with the probability of $p = 0.03$. Thus, dSphs with significantly different stellar mass are likely to have different star formation histories. A similar but less pronounced difference is observed in the cSFHS of dEs. This means that, regardless of morphology, mass is thought to play an important role in the SFHs of early-type dwarfs. The main cause of the difference in the cSFHS between the two mass groups of early-type dwarfs is largely due to the initial explosive bursts of star formation in more massive galaxies. One of the reasons for the less active star formation in the low mass early-type dwarfs seems to be the supernova feedback that removes a large amount of gas left after the initial bursts of star formation. If we consider Figure 13 and Figure 14 together, morphology is, at least, as important as stellar mass for the SFHs of the early-type dwarfs.

4.3.3 Local Background Density

The environment of dwarf galaxies in connection with galaxy morphology has been explored by van den Bergh (1994), Karachentsev, Kaisina & Makarov (2014), and Ann (2017), respectively for the LG, the local volume within 10Mpc, and the local universe $z \lesssim 0.01$. We calculated the local background density (Σ) by the n th nearest neighbor method with $n = 5$ and normalized by their mean values. We used the linking distance of $LD = 1$ Mpc and linking velocity of $\Delta V^* = 1000 \text{ km s}^{-1}$ adopted by Ann (2017). Figure 15 shows the cSFHs as a function of the lookback time for dSphs and dEs in two density groups. As is the case for the dependence on the stellar mass, we used the median (Σ_m) and σ to assign groups. As can be seen, the cSFH of dSphs and dEs in the high density regions is much different from that for the low density regions, for $\log(t_L) > 9.2$. It seems plausible that early-type dwarfs in the high density regions are assembled earlier than those in the low density regions because dynamical time scale such as gravitational collapsing time is inversely proportional to the square root of gas density, i.e., $\tau_{dyn} \sim \rho^{-1/2}$. Galaxies formed in the high density regions collapse more rapidly than those in the low density regions. The local density dependence observed in the cSFHs of dSphs and dEs is understandable if they are formed from the primordial gas clouds which collapse by gravitation. In the earliest phase of galaxy formation at $\log(t_L) \gtrsim 10.1$, the gas cloud out of which the first generation of stars formed collapse more rapidly than those in the low density regions, regardless of their morphology. The initial explosive bursts of star formation observed in dEs seems to be the outcome of the fast collapse at $\log(t_L) \gtrsim 10.1$.

For dEs of primordial origin, the gas out of which stars formed in this period is the gas expelled to the halo by supernova feedback caused by the initial explosive bursts of star formation and accreted to the galaxy after being cooled. In this case, the low background density is more favorable to the gas cooling than the high density regions because interactions with the ambient hot intergalactic medium is less effective in the low density regions. If most of dEs are transformed from late-type galaxies, the opposite trend is expected because gas removal is more effective in the high density regions by ram pressure stripping (Gunn & Gott 1972) which is thought to be the major mechanism to remove the gas from the late-type galaxies. Figure 16 shows the very feature that supports the

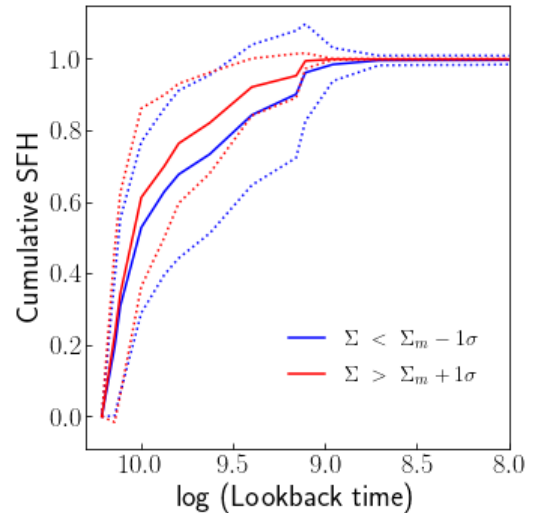


Figure 15. Cumulative SFHs of dSphs and dEs for the low and high background density (Σ). We selected galaxies with Σ less than $\Sigma_m - 1\sigma$ as the low density group and those with Σ greater than $\Sigma_m + 1\sigma$ as the high density group where Σ_m and σ are the median and standard deviation of the local background density of sample galaxies. The solid lines represent the mean cSFHs and the dotted lines are $\pm 1\sigma$ boundaries, blue color for the low density group and red color for the high density group, respectively.

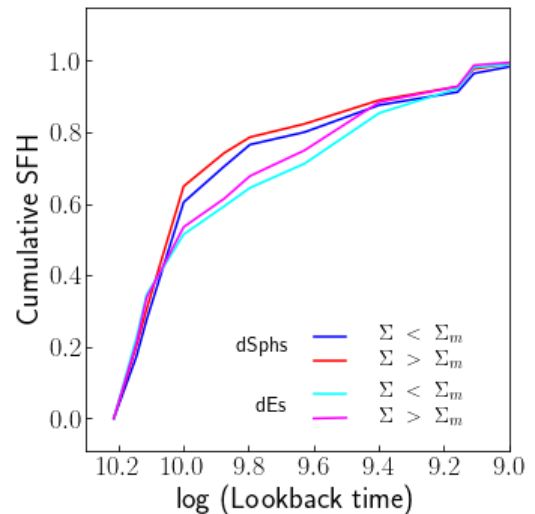


Figure 16. Cumulative SFHs of dSphs and dEs, divided by the local background density (Σ). The low density group has $\Sigma < \Sigma_m$ and the high density group has $\Sigma > \Sigma_m$ where Σ_m is the median Σ of early-type dwarfs. The dSphs of the low density and high density groups are plotted by blue and red lines, respectively, whereas dEs are plotted by cyan and magenta lines, respectively for the low and high density groups.

transformation hypothesis as the origin of dEs although the background density dependence is not statistically significant. Since the difference due to different local background density at fixed morphology is much smaller than the differences due to stellar mass or morphology, it is difficult to exclude the possibility of the primordial origin of dEs.

5 DISCUSSION

5.1 Pre-enrichment and Supernova Feedback

The distinction of dSphs from dEs may help to understand the origin of early-type dwarfs more clearly because their SFHs are significantly different, which implies different origins of dSphs and dEs. The different characteristics of the SFHs of the two sub-types of the early-type dwarfs seems to be closely related to the critical issues on the formation and evolution of galaxies, pre-enrichment and quenching time.

Pre-enrichment of interstellar medium (ISM) and IGM by supernovae from Pop III stars have been thought to be present by simulations (e.g., Brommet et al. 2009) and observations which show absence of extremely low metallicities below $Z \approx 10^{-3} Z_{\odot}$ (Cowie & Songaila 1998; Helmi et al. 2006). The observations that showed a metallicity floor of $\sim 10^{-3} Z_{\odot}$ include the metallicity of the Milky Way halo stars, the LG dSph galaxies (e.g., Helmi et al. 2006), damped Ly α absorption systems (Wolfe & Prochaska 1998), and intervening IGM in the line of sight toward quasars (e.g., Cowie & Songaila 1998). The absence of extremely metal-poor ($Z = 0.0001$) stars among the oldest stellar populations in the majority of the early-type dwarfs (dSphs and dEs) reported here suggests pre-enrichment of the gas out of which the oldest stars formed. The pre-enrichment resulted in the metallicities of the oldest stellar populations as $Z = 0.0004$. This level of pre-enrichment is in good agreement with recent simulations (Tassis, Gnedin & Kravtsov 2012; Wise et al. 2012) in which metals from Pop III supernovae enrich the ISM of the hosting halo and the surrounding IGM.

It is unclear whether the pre-enrichment was made before the collapse of gas into dark matter halo or after the assembly of galaxies. However, the relatively higher metallicity of $Z = 0.0004$ for the first generation of stars in the early-type dwarfs favors in-situ pre-enrichment during the reionization. This scenario is plausible because the inhomogeneous gas surface density could provide a favorable condition for the formation of Pop III stars in the high density pristine gas pockets (Tassis, Gnedin & Kravtsov 2012; Pallottini et al. 2014). However, pre-enrichment before galaxy assembly is not completely excluded because the gas out of which a galaxy formed could be pre-enriched by Pop III stars in the neighboring minihalos. It is also possible that pre-enrichment happened in the subhalos that were merged into the host halo. The ages of the oldest stellar population of dSphs and dEs ($\gtrsim 10$ Gyr) suggest that star formation started just after the end of reionization which is supposed to occur at $z \approx 6$ (Fan, Carilli & Keating 2006).

The violent bursts in $\sim 30\%$ of dSphs and $\sim 35\%$ of dEs at $\log(t_L) > 10$ imply that their mass is larger than the characteristic mass below which star formation is suppressed by the reionization feedback. For the dark matter halo, this characteristic mass M_{halo} is $\sim 10^{10} M_{\odot}$ (Fitts et al. 2017) which corresponds to the virial temperature of $\sim 10^4$ K (Benitez-Llambay et al. 2015). In terms of stellar mass (M_*), it is $\sim 10^6 M_{\odot}$ based on the extrapolated $M_* - M_{halo}$ relation and simulations (Fitts et al. 2017, references there in). These mass scales are consistent with the upper limiting mass of ultra faint dwarfs ($\sim 10^5 M_{\odot}$) whose star formation was quenched by reionization feedback (Rodriguez Wimberly et al. 2019).

There is a signature of severe suppression of star formation in early-type dwarfs due to the feedback of stellar evolution such as supernova explosions in the initial bursts of star for-

mation. This feedback seems to be strong enough to heat the gas left after the initial bursts of star formation and suppresses star formation somewhat before the second peak of star formation at $\log(t_L) = 9.4$. Suppression of star formation after the first period of star formation also seems to be caused by the stellar feedback that heats gas and expels some of them. Removal of gas by supernova feedback seems to be more effective in dSphs because the fraction of stars formed in the second period of star formation is much smaller than those of dEs which show comparable fractions in the first and second period of star formation.

The present sample of early-type dwarfs shows gappy SFHs which are characterized by distinct quiescent periods of star formation (Wright et al. 2019) more frequent than the LG dwarfs (Weisz et al. 2011). In particular, dEs in the present sample show mostly gappy SFHs. Since dEs are, on average, more massive than dSphs, gappy SFHs are likely to be made for galaxies where the supernova feedback is strong enough to heats and expels the gas left to the halos of galaxies but not sufficient to remove the gas to the intergalactic matter. The gas ejected into the halos of galaxies accretes to the galaxies after cooling down and begins to collapse to form next generation of stars. The mass dependent gappy SFH is understandable because the feedback of supernova explosion is more effective in less massive galaxy. In less massive dwarfs, the stellar feedback removes the gas left completely after the first period of star formation.

5.2 Morphology as a fingerprint of the Origin of Early-type dwarfs

From the analysis of SFHs of dSphs and dEs, it seems apparent that the morphology of early-type dwarfs is closely related to their SFHs. As shown in Figure 13, the cSFH of dSphs is clearly different from that of dEs, regardless of their mass. It implies that the morphology dependence of cSFHs seems to be most important in the SFHs of early-type dwarfs (Figures 13 and 14). Thus, dSphs are not merely a faint sub-sample of dEs but are distinct objects. The morphology difference seems to be due to their different origins. The majority of dSphs are likely to be primordial objects while most dEs are likely to be transformed ones. It is more likely that most faint dSphs are originated from the primordial objects some of which are collapsed before reionization while the majority of bright dEs are transformed from the late-type galaxies as implied by the embedded spiral arms in a number of dEs (Lisker, Grebel & Binggeli 2006; Seo & Ann 2022). However, it is highly plausible that some fractions of dEs are primordial objects, in particular, the dEs of which quenching of star formation occurred before $\log(t_L) \approx 10$. On the other hand, the origin of some dSphs whose star formation quenched after $\log(t_L) \approx 9.7$ is not clear. They can be primordial objects as well as transformed ones. If they are primordial objects, the delayed quenching of star formation needs to be explained.

The terminology of fast dwarfs and slow dwarfs were introduced by Gallart et al. (2015) to distinguish cSFHs of dwarf galaxies. On average, the present sample of dSphs and dEs are said to be slow dwarfs because the mean cSFHs at $\log(t_L) \approx 10$ are 0.65 and 0.54 for dSphs and dEs, respectively. However, there are a number of fast dwarfs in the present sample. In particular, a significant fraction of dSphs are fast dwarfs if we consider that dwarfs that quenches at $\log(t_L) \approx 10$ or

redshift of $z \sim 2$, are fast dwarfs. Since most star formation occurred before $\log(t_L) = 10$, fast dwarfs are thought to be primordial objects.

There seems to be a trend between the mass of a galaxy and τ_{90} . Less massive dwarfs are likely to be fast dwarfs (Weisz et al. 2014a,b) and they are considered to be fossils of reionization which formed the bulk of its stars prior to reionization (Weisz et al. 2014b). The dependence of τ_{90} on the mass of a galaxy is consistent with the recent simulations of Digby et al. (2019). The fact that fast dwarfs are more frequent in dSphs than in dEs is consistent with the dependence of quenching time on the stellar mass because dEs are on average ~ 4 times more massive than dSphs. Some fast dSphs could be fossils of reionization if the bulk of their stars were formed prior to reionization. The suppression of star formation which resulted in almost complete quenching of star formation in the majority of dSphs after $\log(t_L) \approx 10$ is caused by the feedback from supernova explosions. But, the suppression after the initial bursts in dSphs and dEs at $\log(t_L) > 10$ could be caused by reionization or feedback from supernova explosions because both of them depend on the galaxy mass. It is well known that suppression or quenching of star formation by reionization are thought to be effective for lower mass dwarfs (Gnedin 2000; Bovill & Ricotti 2009; Benitez-Llambay et al. 2015; Jeon, Besla & Bromm 2017; Dawoodbhoy et al. 2018). The difference between the SFHs of the two sub-types of early-type dwarfs are thought to be mainly due to their difference in origin.

The pronounced differences in SFHs between dSphs and dEs are the paucity of moderately old (~ 2.5 Gyr) stars in dSphs. It is thought to be caused by the effects of reionization and feedback from supernova explosion which expel gas left into the halo of the galaxy. It is also the reason why the chemical evolution of dSphs was suppressed. These ejected gas evaporated from the halo and some remained there. Since the gas ejected into the halo was enriched before being expelled, this enriched gas can be mixed with the IGM around the galaxy. The rapid chemical evolution in dEs was possible due to the relatively large mass which prevented the removal of gas at early epochs when reionization and supernova feedback were strong. During the second period of star formation between $\log(t_L) \approx 9.7$ and 9, the metal content of gas out of which the moderately old stars were formed increased monotonically. The monotonic increase of metallicity in the second period of star formation can be explained by a simple chemical evolution model which assumes a closed box with a reservoir such as that of Hartwick (1976). Here, the halo played the role of a reservoir.

6 SUMMARY AND CONCLUSIONS

We have analyzed the SDSS spectra to derive the SFHs of 200 dSphs and 234 dEs of which morphology is classified by Ann, Seo & Ha (2015). On average, dSphs in the present sample is 1.5 mag fainter than dEs. We used a population synthesis code STARLIGHT (Cid Fernandes et al. 2005). The SFHs of dSphs and dEs show observational evidences related to the reionization of the Universe and the stellar feedback. They are pre-enrichment and early quenching of star formation in a significant fraction of early-type dwarfs. The early quenching is more pronounced in dSphs than dEs due to smaller

mass of dSphs. Pre-enrichment of the oldest stellar populations formed at $\log(t_L) > 10$ made the metallicity of the oldest stellar population as high as $Z=0.0004$. The non-zero metallicity of the oldest stellar populations is thought to be enriched by PoP III stars during the reionization.

Owing to the energy input from the supernova feedback, there is a period of weakly suppressed star formation in a significant fraction of dSphs and dEs after the initial bursts of star formation at $\log(t_L) > 10$. The gradual increase of metallicity, from $Z = 0.0004$ to $Z = 0.05$, seen in the stellar populations of dEs which formed until $\log(t_L) \approx 9$ reflects the homogeneous mixing of metals in the remaining gas of dEs. In contrast, the star formation in dSphs is almost completely suppressed due to supernova feedback that removes the gas from the central regions. The gas left after the first period of starbursts is expelled to the halo and some heated gas would be evaporated. It resulted in the paucity of moderately old, intermediate-metallicity stars in dSphs.

The SFH of dEs is characterized by two comparable peaks of active star formation while the SFH of dSphs shows a prominent peak at $\log(t_L) = 10$ with a small bump at $\log(t_L) = 9.4$. It means that dEs have two periods of active star formation with a gap between them. The reason for the lack of second peak in the SFH of dSphs is the supernova feedback that expels the gas left into the halo of the galaxy or outside the halo. In contrast, dEs can keep a significant amount of gas left for star formation. But it takes time for the gas to cool sufficiently and collapse. This is the reason why there is a gap between the two peaks in the SFH of dEs.

The SFHs of galaxies are thought to be affected by the internal properties of galaxies as well as their environment. There is a significant difference in the cSFHs between the early-type dwarfs in the low density regions and those in the high density regions. But if we fix the morphology, the difference between the two density groups decreases significantly although the same trend is maintained. The density dependence of cSFHs of early-type dwarfs is consistent with the dependence of the dynamical times on the local background density. The morphology of early-type dwarfs is thought to be, at least, as important as the stellar mass for the SFHs of the early-type dwarfs. Morphology reflects their SFHs while the stellar mass seems to drive star formation, especially in galaxies with primordial origin. This is the reason why the effect of stellar mass is more pronounced in dSphs which are thought to be mostly primordial objects.

It is of worth to distinguish dSphs from dEs in morphology classification of early-type dwarf galaxies since their SFHs are clearly different. The difference in SFHs of dSphs and dEs seems to be closely related to their origin, The majority of dSphs are thought to be primordial origin while the majority of dEs are transformed ones.

ACKNOWLEDGMENTS

Authors would like to thank the anonymous reviewer whose comments and suggestions greatly improve the present paper. This work was supported partially by the NRF Research grant 2015R1D1A1A09057394.

DATA AVAILABILITY

The original data underlying this article are available in SDSS DR7. We provide the basic output of STARLIGHT as supplemented materials and additional data are available upon request.

REFERENCES

- Abadi, M. G., Moore, B., Bower, R. G., 1999, *MNRAS*, 308, 947
 Ann, H. B., Seo, M., Ha, D. K., 2015, *ApJS*, 217, 27
 Ann, H. B., 2017, *JKAS*, 50,111
 Aparicio, A., Carrera, R., Martínez-Delgado, D., 2001, *AJ*, 122, 2524
 Assmann, P., Fellhauer, M., Wilkinson, M. I., Smith, R., 2103, *MNRAS*, 432, 274
 Barazza, F. D., Binggeli, B., Jerjen, H., 2002, *A&A*, 391, 831
 Bacon, R., et al., 2010, in McLean I. S., Ramsay S. K., Takami H., eds, *Proc. SPIE Conf. Ser. Vol. 7735, Ground-based and Airborne Instrumentation for Astronomy III*. SPIE, Bellingham, p. 773508
 Barkana, R., Loeb, A., 1999, *ApJ*, 523, 54
 Barmantloo, S., Cautun, M., 2023, *MNRAS*, 520, 1704
 Becker, R. H., Fan, X., White, R. L. et al., 2001, *AJ*, 122, 2850
 Benitez-Llambay, A., Navarro, J. F., Abadi, M. G., Gottlöber, S., Yepes, G., Hoffman, Y., Steinmetz, M., 2013, *ApJ*, 763, L41
 Benitez-Llambay, A., Navarro, J. F., Abadi, M. G., Gottlöber, S., Yepes, G., Hoffman, Y., Steinmetz, M., 2015, *MNRAS*, 450, 4207
 Bettinelli, M., Hidalgo, S. L., Cassisi, S., Aparicio, A., Piotto, G., 2018, *MNRAS*, 476, 718
 Bettinelli, M., Hidalgo, S. L., Cassisi, S., Aparicio, A., Piotto, G., Valdes, F., Walker, A. R., 2019, *MNRAS*, 487, 5862
 Binggeli, B., Sandage, A., & Tammann, G. A. 1985, *AJ*, 90, 1681
 Blumenthal, G. R., Faber, S. M., Primack, J. R., Rees, M. J., 1985, *Nature*, 313, 72
 Boselli, A., Boissier, S., Cortese, L., Gavazzi, G. 2008, *ApJ*, 674, 74
 Bovill, M. S., Ricotti, M., 2009, *ApJ*, 693, 1859
 Bressanm A., et al., 2012, *MNRAS*, 427, 127
 Brinchmann, J., Charlot, S., White, S. D. M., Tremonti, C., Kauffmann, G., Heckman, T., Brinkmann, J., 2004, *MNRAS*, 351, 1151
 Brown, T. M., et al., 2014, *ApJ*, 796, 91
 Bromm, V., Yoshida, N., Hernquist, L., McKee, C. F., 2009, *Nature*, 459, 498
 Bruzual, G., Charlot, S., 2003, *MNRAS*, 344, 1000
 Bundy, K., et al., 2015, *ApJ*, 798, 7
 Buta, R. J., et al., 2015, *ApJS*, 217, 32
 Buyle, P., De Rijcke, S., Michielsen, D., Baes, M., Dejonghe, H., 2005, *MNRAS*, 360, 853
 Cardelli, J. A., Clayton, G. C., Mathis, J. S., 1980, *ApJ*, 345, 245
 Carrera, R., Aparicio, A., Martínez-Delgado, D., Alonso-García, J., 2002, *AJ*, 123, 3199
 Chabrier G., 2003, *PASP*, 115, 763
 Choi, Y.-Y., Han, D.-H., Kim, S. S., 2010, *JKAS*, 43, 191
 Chilingarian, I., Cayatte, V., Revaz, Y., Dodonov, S., Durand, D., Durret, F., Micol, A., Slezak, E., 2009, *Sci*, 326, 1379
 Cid Fernandes, R., Gonzalez. D. R. M., Schmitt, H., Storchi-Bergmann, T., Martins, L. P., Perez, E., Heckman, T., Leitherer, C., Schaerer, D., *ApJ*, 605, 105
 Cid Fernandes, R., Mateus, A., Sodre, L., Stasiriska, G., Gomes, J. M., 2005, *MNRAS*, 358, 363
 Cid Fernandes, R., et al., 2013, *A&A*, 557, 86
 Cid Fernandes, R., 2018, *MNRAS*, 480, 4480
 Cignoni, M., et al., 2019, *ApJ*, 887, 112
 Conselice, C., O’Neil, K., Gallagher, J., Wyse, R., 2003, *ApJ*, 591, 167
 Cowie, L. L., Songaila, A., 1998, *Nature*, 394, 44
 D’Souza R., Bell E. F., 2021, *MNRAS*, 504, 5270
 Danforth, C. W., Shull, J. M., 2008, *ApJ*, 679, 194
 Dawoodbhoy, T., et al., 2018, *MNRAS*, 480, 1740
 de Boer, T. J. L., Tolstoy, E., Hill, V., Saha, A., Olszewski, E. W., Mateo, M., Starkenburg, E., Battaglia, G., Walker, M. G., 2012, *A&A*, 544, 73
 De Rijcke, S., Dejonghe, H., Zeilinger, W. W., Hau, G. K. T., 2003, *A&A*, 119, 125
 De Rijcke, S., Michielsen, D., Dejonghe, H., Zeilinger, W. W., & Hau, G. K. T., 2005, *A&A*, 438, 491
 Dekel A., Silk J., 1986, *ApJ*, 303, 39
 Digby, R., Navarro, J. F., Fattahi, A., Simpson, C. M., Oman, K. A., Gomez, F. A., Frenk, C. S., Grand, R. J. J., Pakmor, R., 2019, *MNRAS*, 485, 5423
 Dolphin, A. E., 2002, *MNRAS*, 332,91
 Emerick, A., Bryan, G. L., Mac Low, M.-M., 2019, *MNRAS*, 482, 1304
 Fan, Xiaohui, Carilli, C. L., Keating, B., 2006, *ARA&A*, 44, 41
 Fattahi, A., Navarro, J. F., Frenk, C. S., Oman, K. A., Sawala, T., Schaller, M., 2018, *MNRAS*, 476, 3816
 Ferrara, A., Tolstoy, E., 2000, *MNRAS*, 313, 291
 Fitts, A., et al., 2017, *MNRAS*, 472, 2945
 Frebel, A., Simon, J. D., Kirby, E. N., 2014, *ApJ*, 786, 74
 Gallagher, J. S. III, Wyse, R. F. G., 1994, *PASP*, 106, 1225
 Gallazzi, A., Charlot, S., Brinchmann, J., White, S. D. M., Tremonti, C., A2006, *MNRAS*, 362, 41
 Gallazzi, A., Brinchmann, J., Charlot, S., White, S. D. M., 2008, *MNRAS*, 383, 1439
 Gallart, C., et al., 2015, *ApJ*, 811, L18
 Gallart, C., et al., 2021, *ApJ*, 909, 192
 Garrison-Kimmel, S., et al., 2019, *MNRAS*, 489, 45
 Geha, M., Guhathakurta, P., van der Marel, R. P., 2002, *AJ*, 124, 3087
 Geha, M., Guhathakurta, P., van der Marel, R. P., 2003, *ApJ*, 126, 1794
 Geha, M., van der Marel, R. P., Guhathakurta, P., Gilbert, K. M., Kalirai, J., Kirby, E. N., 2010, *ApJ*, 711, 361
 Gnedin, N. Y., 2000, *ApJ*, 542, 535
 Grebel, E. S., GaLLagher, J. S. III, Harbeck, D., 2003, *AJ*, 125, 1926
 Graham, A. W. Jerjen, H., Guzman, R., 2003, *AJ*, 126, 1787
 Graham, A. W., 2019, *MNRAS*, 487, 4999
 Gunn J. E., Gott, III J. R., 1972, *ApJ*, 176, 1
 Gutcke, Thales A., Pfrommer, C., Bryan, G. L., Pakmor, R., Springel, V., Naab, T., 2022, *ApJ*, 941, 120
 Hallenbeck, G., et al., 2012, *AJ*, 144, 87
 Hammer, F., et al., 2023, *MNRAS*, 519, 5059
 Hamraz, E., et al., 2019, *A&A*, 625, 94
 Hartwick, F. D. A., 1876, *ApJ*, 209, 418
 Helmi, A. Irwin, M. J., Tolstoy, E., et al., 2006, *ApJ*, 651, L12
 Hernandez, X., Gilmore, G., Valls-Gabaud, D., 2000, *MNRAS*, 317, 8
 Hidalgo, S. L., 2012, *ASP Conference Series*, 458, 287
 Hidalgo, S. L., et al., 2013, *ApJ*, 778, 103
 Jeon, M., Besla, G., Bromm, V., 2017, *ApJ*, 848, 85
 Jerjen, H., Kalnajs, A., Binggeli, B., 2000, *A&A*, 358, 849
 Joshi, G. D., Pillepich, A., Nelson, D., Zinger, E., Marinacci, F., Springel, V., Vogelsberger, M., Hernquist, L., 2021, *MNRAS*, 508, 1652
 Karachentsev, I. D., Makarov, D. I., 2013, *AJ*, 145, 101
 Karachentsev, I. D., Kaisina, E. I., Makarov, D. I., 2013, *AJ*, 147, 13
 Kazantzidis, S., Mayer, L., Callegari, S., Dotti, M., Moustakas, L. A., 2017, *ApJ*, 836, L13
 Kauffmann, G., et al., 2003, *MNRAS*, 341, 33

- Koppen, J., Jachym, P., Taylor, R., Palouš, J., 2018, MNRAS, 479, 436
- Kravtsov, A. V., Gnedin, O. Y., Klypin, A. A., 2004, ApJ, 609, 482
- Kormendy, J., Bender, R., 2012, ApJS, 198, 2
- Larson, R., Tinsley, B., Caldwell, N., 1980, ApJ, 237, 69
- Le Borgne J.-F. et al., 2003, A&A, 402, 433
- Lee, M. G., Yuk, I.-S., Park, H. S., Harris, J., Zaritsky, D., 2009, ApJ, 703, 692
- Lisker, T., Grebel, E. K., Binggeli, B., 2006, AJ, 132, 497
- Lisker, T., Grebel, E. K., Binggeli, B., Glatt, K., 2007, ApJ, 660, 1186
- Lokas, E. L., Ebrova, I., del Pino, A., Semczuk, M., 2014b, MNRAS, 445, L6
- Makarov, D. I., Sharina, M. E., Karachentseva, V. E., Karachentseva, I. G., 2015, A&A, 581, 82
- Makarova, L. N., Makarov, D. I., Karachentsev, I. D., Tully, R. B., Rizzi, L., 2017, MNRAS, 464, 2281
- Monelli, M., et al., 2010a, ApJ, 720, 1225
- Monelli, M., et al., 2010b, ApJ, 722, 1864
- Marcolini, A., D’Ercole, A., Brighenti, F., Recchi, S., 2006, MNRAS, 371, 643
- Mayer, L., Governato, F., Colpi, M., Moore, B., Quinn, T., Wadsley, J., Stadel, J., Lake, G., 2001, ApJ, 547, L123
- Mayer, L., Governato, F., Colpi, M., Moore, B., Quinn, T., Wadsley, J., Stadel, J., Lake, G., 2001, ApJ, 559, 754
- McConnachie, A. W., AJ, 144, 4
- Moore, B., Katz N., Lake, G., Dressler, A., Oemler, A., 1996, Nature, 379, 613
- Moore, B., Lake, G., Katz, N., 1998, ApJ, 495, 139
- Muller, O., et al., 2021, A&A, 645, 92
- Navabi, M., et al., 2021, ApJ, 910, 127
- Navarro, J. F., Frenk, C. S., White, S. D. M., 1997, ApJ, 490, 493
- Pallottini, A., Ferrara, A., Gallerani, S., Salvadori, S., D’Odorico, V., 2014, 2014, MNRAS, 440, 2498
- Paudel, S., Ree, C. H., 2014, ApJ, 796, L14
- Pedraz, S., Gorgas, J., Cardiel, N., Sanchez-Blazquez, P., Guzman, R., 2002, MNRAS, 332, L59
- Penny, S. J., Pimblet, K. A., Conselice, C. J., Brown, M. J. I., Grützbauch, R., Floyd, D. J. E., 2012, ApJ, 758, 32
- Penny, S. J., Masters, K. L., Weijmans, A.-M., et al. 2016, MNRAS, 462, 3955
- Riffel, R., et al., 2021, MNRAS, 501, 406
- Rodriguez Wimberly, M. K., Cooper, M. C., Fillingham, S. P., Boylan-Kolchin, M., Bullock, J. S., Garrison-Kimmel, S., 2019, MNRAS, 483, 403
- Rusakov, V., et al., 2021, MNRAS, 502, 6
- Salucci, P., et al., 2012, MNRAS, 420, 20
- Sanchez, S. F., Kennicutt, R. C., Gil de Paz, A., et al. 2012, A&A, 538, A8
- Santana, F. A., et al., 2016, ApJ, 829, 863
- Savino, A., Salaris, M., Tolstoy, E., A&A, 583, 126
- Savino, A., Tolstoy, E., Salaris, M., Monelli, M., de Boer, T. J. L., 2019, A&A, 630, 116
- Salvadori, S., Ferrara, A., Schneider, R., 2008, MNRAS, 386, 348
- Sandage, A., Binggeli, B., 1984, AJ, 89, 919
- Seo, M., Ann, H. B., 2022, MNRAS, 514, 5853
- Sérsic, J. L., 1968, Atlas de Galaxias Australes (Cordoba: Observatorio Astronomico)
- Schlegel, D., Finkbeiner, D. P., Davis, M., 1998, ApJ, 500, 525
- Shapiro, P. R., Iliev, I. T., Raga, A. C., 2004, MNRAS, 348, 753
- Simien, F., Prugniel, P., 2002, A&A, 384, 371
- Skillman, E. D., et al., 2017, ApJ, 837, 102
- [Strateva, I., et al., 2001, AJ, 122, 1861
- Tassis, K., Gnedin, N. Y., Kravtsov, A. V., 2012, ApJ, 745, 68
- Toloba, E., Guhathakurta, P., Boselli, A., et al. 2015, ApJ, 799, 172
- Tolstoy, E., Hill, V., Tosi, M., 2009, ARA&A, 47, 371
- Vader, J. P., 1986, ApJ, 305, 889
- van den Bergh, S., 1976, ApJ, 206, 883
- van den Bergh, S. 1994, ApJ, 428, 617
- van Zee, L., Skillman, E. D., Haynes, M. P., 2004, AJ, 128, 121
- Wakker, B. P., Savage, B. D., 2009, ApJS, 182, 378
- Walker, M. G., Mateo, M., Olszewski, E. W., Penarruria, J., Evans, N. W., Gilmore, G., 2009, 704, 127
- Wang, J., et al., 2022, ApJ, 258, 9
- Webster D., Frebel, A., Bland-Hawthorn, J., 2016, ApJ, 818, 80
- Weisz, D. R., et al. 2011, ApJ, 739, 5
- Weisz, D. R., Dolphin, A. E., Skillman, E. D., Holtzman, J., Gilbert, K. M., Dalcanton, J. J., Williams, B. F., 2014a, ApJ, 789, 147
- Weisz, D. R., Dolphin, A. E., Skillman, E. D., Holtzman, J., Gilbert, K. M., Dalcanton, J. J., Williams, B. F., 2014b, ApJ, 789, 148
- Weisz, D. R., Dolphin, A. E., Skillman, E. D., Holtzman, J., Gilbert, K. M., Dalcanton, J. J., Williams, B. F., 2015, ApJ, 804, 136
- Weisz, D. R., et al., 2019, ApJ, 885, L8
- Wheeler, C., Pace, A. B., Bullock, J. S., et al., 2017, MNRAS, 465, 2420
- Wise, J. H., Turk, M. J., Norman, M. L., Abel, T., 2012, ApJ, 745, 50
- Wolfe, A. M., Prochaska, J. X., 1998, ApJ, 494, L15
- Wright, A. C., Brooks, A. M., Weisz, D. R., Christensen, C. R., 2019, MNRAS, 482, 1176
- York, D. G., et al. 2000, AJ, 120, 1579
- Zhou, S., Mo, H. J., Li, C., Boquien, M., Rossi, G., 2020, MNRAS, 497, 47

This paper has been typeset from a $\text{\TeX}/\text{\LaTeX}$ file prepared by the author.